論文 / 著書情報
Article / Book Information

Title	Continuous-wave operation of a 1.3 μm wavelength npn AlGaInAs/InP transistor laser up to 90 °C
Author	Shoichi Yoshitomi, Kentarou Yamanaka, Yusei Goto, Yuta Yokomura, Nobuhiko Nishiyama, Shigehisa Arai
Citation	Japanese Journal of Applied Physics, Vol. 59, Number 4, p. 042003
Pub. date	2020, 4
DOI	10.35848/1347-4065/ab7ef2
Creative Commons	Information is in the article.

Japanese Journal of Applied Physics

The Japan Society of Applied Physics

REGULAR PAPER • OPEN ACCESS

Continuous-wave operation of a 1.3 μm wavelength npn AlGaInAs/InP transistor laser up to 90 °C

OPEN ACCESS

Japanese Journal of Applied Physics **59**, 042003 (2020) **REGULAR PAPER**

https://doi.org/10.35848/1347-4065/ab7ef2

Continuous-wave operation of a 1.3 μm wavelength npn AlGaInAs/InP transistor laser up to 90 °C

S. Yoshitomi[1], K. Yamanaka[1], Y. Goto[1], Y. Yokomura[1], N. Nishiyama[1,2*], and S. Arai[1,2]

[1]*Department of Electrical and Electronic Engineering, Tokyo Institute of Technology, 2-12-1 O-okayama, Meguro-ku, Tokyo 152-8552, Japan*
[2]*Institute of Innovative Research (IIR), Tokyo Institute of Technology, 2-12-1 O-okayama, Meguro-ku, Tokyo 152-8552, Japan*

*E-mail: nishiyama@ee.e.titech.ac.jp

Received December 12, 2019; revised February 22, 2020; accepted March 11, 2020; published online April 2, 2020

A transistor laser (TL) is a device that operates at a high-speed with multiple functions such as output control with low wavelength shift and signal mixing. By adopting a high heat dissipation structure with a high-speed compatible wide electrode pad and thick Au plating in TLs, improvement of temperature performance in 1.3 μm wavelength npn AlGaInAs/InP TL was demonstrated. As a result, continuous-wave operation of a 1.3 μm TL up to 90 °C was achieved. The thermal resistance was estimated to be 25 K W^{-1}, based on the spectrum behavior, which is at least four times lower than the previously observed value. © 2020 The Japan Society of Applied Physics

1. Introduction

Recently, the internet traffic in data centers has been increasing substantially due to an increase in the number of internet users and the spread of telecommunication equipment such as smartphones and tablets. Accordingly, there is a need for high-speed optical communication. Directly modulated laser diodes (DMLs) are commonly used for short to medium distance optical communication systems. DMLs are superior in terms of low power consumption and small footprint. However, their modulation speeds are limited to around 50 Gbaud owing to the damping effect[1,2] and direct modulation at 50 Gbps has been reported.[3] Therefore, new high-speed optical sources are necessary for replacing conventional DMLs. The transistor laser (TL) was proposed[4] as a candidate to overcome the modulation speed limit of DMLs.[5–7] The TL is a simple device based on a heterojunction bipolar transistor[8] with an active layer in the base region. Unlike conventional laser diodes, the TL has three-terminals viz. emitter, base, and collector. Thanks to this unique configuration, the TL is capable of both current and voltage modulation. The combination of these two modulation methods can lead to multiple functions such as output control with low wavelength shift[9] and signal mixing.[10] Based on theoretical calculations, it is expected that a high-speed modulation exceeding the limit of conventional DMLs is possible for both cases.[7,11,12] Indeed, both voltage and current modulation at 20 Gbps and room temperature were demonstrated using TLs operating at a wavelength of 1 μm or shorter.[13] For long-wavelength TLs, we have demonstrated continuous-wave (CW) operation of 1.3 μm npn AlGaInAs/InP TLs, fabricated on InP substrates[14–19] and CW operation of 1.5 μm wavelength GaInAsP/InP TLs has already been demonstrated.[20] However, the maximum operation temperature of long-wavelength TLs were limited up to 40 °C. High temperature operation enables both low power consumption and a smaller footprint through uncooled operation.[21] High-speed operation of long-wavelength TLs has not yet been realized mainly due to a large parasitic capacitance. In the previous conference, we briefly reported improved temperature characteristics of 1.3 μm wavelength TLs.[22] In this paper, we report the detail characteristics of highest CW operation temperature of 90 °C for 1.3 μm wavelength TLs by adopting a high heat dissipation structure. In the Sect. 2, the device structure and fabrication are explained. In the Sect. 3, the device characteristics including high temperature characteristics are shown.

2. Device structure and fabrication

Figure 1 shows a cross-sectional view of the TL. Pyramidal type mesa structure with three different mesa width was formed. And we would like to name these three mesas as collector mesa, base mesa and emitter mesa, respectively, from the top. Five strain-compensated AlGaInAs QWs (well width of 5 nm, barrier width of 10 nm, and total thickness of 85 nm) were employed as the active layer to operate at 1.3 μm wavelength with better high temperature characteristics.[23] A graded-index separate confinement heterostructure (GRIN-SCH), whose composition was changed from AlGaInAs (band gap or $E_g = 1.17$ eV at 300 K) to AlInAs ($E_g = 1.46$ eV at 300 K), was used for both sides of the active layer. The thickness of these layers was ~100 nm on the n-side and ~80 nm on the p-side. A buried heterostructure (BH) with n/p/n/p-InP was used to obtain high optical and carrier confinement. The width of p-GaInAsP base layer was chosen to be as narrow as the width of the collector mesa in order to suppress non-radiative recombination in the base layer. A 3.5 μm thick Au electrode pattern was formed on the top of each mesa. The pattern on the base electrode was fabricated to be wide enough in the lateral direction in order to facilitate high heat dissipation. The device was bonded onto an AlN submount, which has high thermal conductivity, by soldering.

The fabrication process of the TL is as follows. At first, an initial wafer containing five AlGaInAs QWs was grown on a Fe-doped (100) semi-insulating InP substrate by using organometallic vapor-phase epitaxy. Next, a stripe mesa was formed by Br_2/CH_3OH wet etching and CH_4/H_2 reactive ion etching. Following in situ thermal cleaning under PH_3 atmosphere, for removing the oxidized surface, a n/p/n/p-InP thyristor structure was deposited for current blocking as well we optical confinement.[24–27] Please note the stripe width of

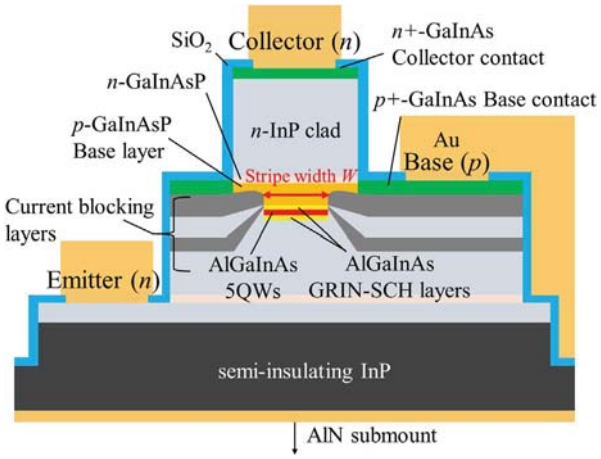

Fig. 1. (Color online) Structure of a npn-AlGaInAs/InP TL.

W is defined as this metsa width (the width of QWs). Subsequently, a p-GaInAsP base layer (100 nm, $E_g = 1.03$ eV) and a n-GaInAsP layer (40 nm, $E_g = 1.03$ eV) were grown and etched at both sides of the stripe by SiO_2 mask. Using this SiO_2 mask, a p^+-GaInAs base contact layer (100 nm) was selectively grown on both sides of the stripe. Next, a n-InP sub-collector layer (2 μm) and a n+-GaInAs collector contact layer (50 nm) were grown. After this regrowth, collector, base, and emitter mesas were formed by etching and SiO_2 (100 nm) was deposited on the surface as an insulating layer. Then, the electrodes were formed by evaporating Ti/Pt/Au on the device. Also, the base electrode was widened and deposited on the side of base mesa in order to facilitate better heat dissipation in the lateral direction of the active layer in addition to making the device compatible for modulation measurements, which means this electrode was designed under consideration of RF characteristics with direct probing of GSG high-speed probe. Finally, a 3.5 μm thick Au layer was deposited by electrolytic plating (plating rate of 15 nm min^{-1}) on the electrodes as a heat spreader.[28] Au plating pattern was formed using a lift-off process. Then, the wafer was made thinner (<200 μm) using lapping process. After cleaving the wafer to form Fabry–Pèrot cavities with a length of 300–1000 μm, devices were bonded onto an AlN submount by soldering. An optical microscope top view and a scanning electron microscope (SEM) cross-sectional view of fabricated TLs are shown in Figs. 2 and 3, respectively. As described above, a wide base electrode pattern (30 μm on the base mesa and 130 μm on the

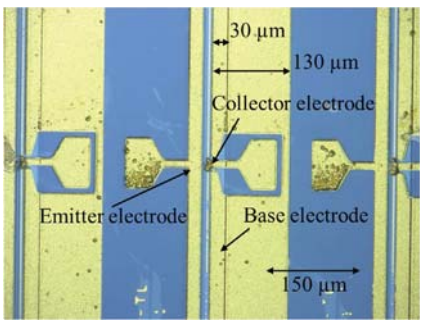

Fig. 2. (Color online) Optical microscope top view of the fabricated device.

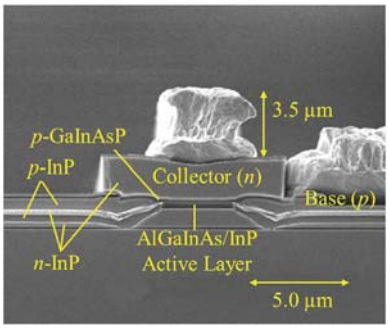

Fig. 3. (Color online) SEM cross-sectional view of the fabricated device.

Fe-InP substrate) and a thick Au plating was introduced to eliminate heat from the active region as well as realize enough heat capacity.

3. Device characteristics

Figure 4 shows both the base current versus the light output power (I_B–P) and the base current versus the collector current (I_B–I_C) characteristics for various collector-emitter voltages (V_{CE}) in a common emitter configuration under room temperature CW (RT–CW at 20 °C) condition. We used a current source and a voltage source for controlling the base current I_B and the collector-emitter voltage V_{CE}, respectively. The cavity length and the stripe width were 490 μm and 1.2 μm, respectively. At $V_{CE} = 4$ V, the threshold base current (I_{Bth}) was 13 mA (corresponding to a threshold current density of 2.2 kA cm^{-2}) and the differential quantum efficiency (η_d) for both facets was 23%. The threshold current density was reduced by 15% compared to a previously reported device[29] due to the introduction of GRIN-SCH. When V_{CE} was applied, undesired recombination in the p-GaInAsP base layer was suppressed because some electrons were withdrawn by the collector and desired recombination occurred in the QWs. At the same time, the optical absorption coefficient of the p-n junction between the collector and the base was increased due to the Franz–Keldysh (FK) effect. Therefore, the light output power saturated with a change in V_{CE}.

Figure 5 shows both the emitter current versus the light output power (I_E–P) and the emitter current versus the collector current (I_E–I_C) characteristics for various

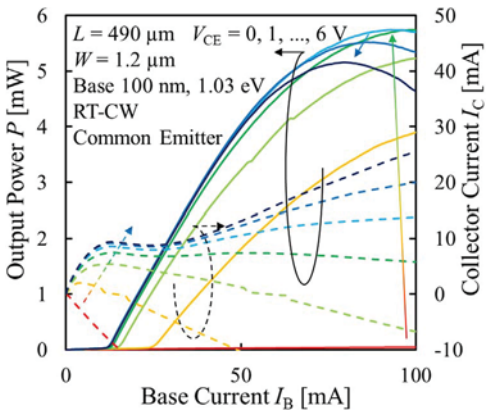

Fig. 4. (Color online) I_B–P (Solid lines) and I_B–I_C (Dotted Lines) characteristics in the common emitter configuration. Each color of lines indicates the characteristics with different V_{CE} (0 V to 6 V with 1 V step, the arrow direction shows the direction of increment).

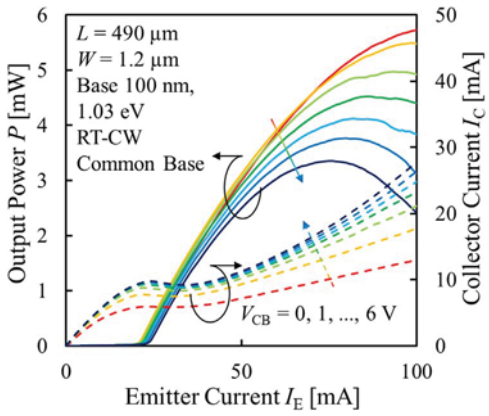

Fig. 5. (Color online) I_E–P (Solid lines) and I_E–I_C (Dotted Lines) characteristics in the common base configuration. Each color of lines indicates the characteristics with different V_{CE} (0 V to 6 V with 1 V step, the arrow direction shows the direction of increment).

collector-base voltages (V_{CB}) in a common base configuration under RT–CW condition. We used a current source and a voltage source for controlling the emitter current I_E and the collector-base voltage V_{CB}, respectively. The device was the same as the one used in Fig. 4. At $V_{CB} = 0$ V, the threshold emitter current (I_{Eth}) was 22 mA (corresponding to a threshold current density of 3.7 kA cm^{-2}) and the η_d for both facets was 23%. The light output power was observed to decrease with increasing V_{CB}, which may be attributed to the FK effect and the Early effect. While the optical absorption coefficient was increased due to the FK effect upon the application of V_{CB}, the number of electrons flowing to the collector was increased because of the Early effect. Figure 6 shows cavity length dependence of $1/\eta_d$ for various V_{CB} in the common base configuration under RT-CW condition. The stripe width was 2.2 μm. Upon increasing V_{CB} from 0 to 6 V, a concomitant increase in the waveguide loss was observed from 11 to 14 cm^{-1}. This observation implies that the FK effect increases with V_{CB}.

The thermal resistance was also measured from the spectrum behavior under various biases and temperatures[30] with a two-terminal base-emitter configuration having a floating collector. Figure 7 shows the wavelength dependence on the dissipated power under CW operation. The dissipated power was defined as the difference between the applied power and light output power. The cavity length and the stripe width of the TL were 1000 μm and 1.2 μm, respectively. The $\Delta\lambda/\Delta P_{diss}$ value of the TL was 0.0021 nm mW^{-1}. In addition, the wavelength dependence on the heat sink temperature was measured under pulse operation (pulse width of 1.0 μs, duty cycle of 0.1%). The $\Delta\lambda/\Delta T$ value of the TL was 0.085 nm K^{-1}. The thermal resistance was calculated to be 25 K W^{-1}, which was much lower than the previously reported value (110 K W^{-1}) of the device without wide electrode pattern and an AlN submount.[19]

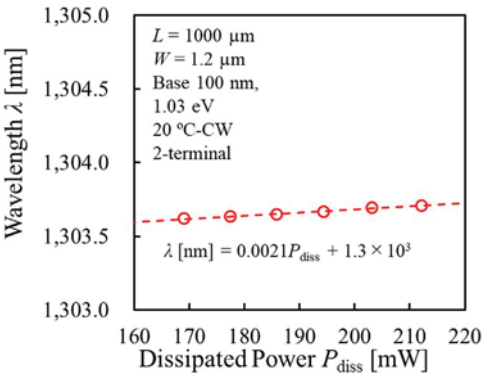

Fig. 7. (Color online) Wavelength dependence on the dissipated power.

Figure 8 shows the light output characteristics at various temperatures in a two-terminal configuration. The cavity length and the stripe width were 1000 μm and 1.2 μm, respectively. At 20 °C, the threshold current was 29 mA while the η_d for both facets was 21%. The CW operation up to 90 °C was successfully achieved. To the best of our knowledge, this is the highest CW operation temperature reported yet for long-wavelength TLs. The low value of R_{th} and high-temperature CW operation may be attributed to both better BH and improved heat dissipation structures.

4. Conclusion

In conclusion, 1.3 μm wavelength TLs with a high heat dissipation structure were fabricated. A thermal resistance of 25 K W^{-1} that is at least four times lower than previously reported values was obtained. More importantly, the CW operation of TL at a temperature of 90 °C was successfully demonstrated. This is the highest CW operation temperature reported thus far for long-wavelength TLs. This result can lead to low power consumption and a smaller footprint for long-wavelength TLs through uncooled operation.

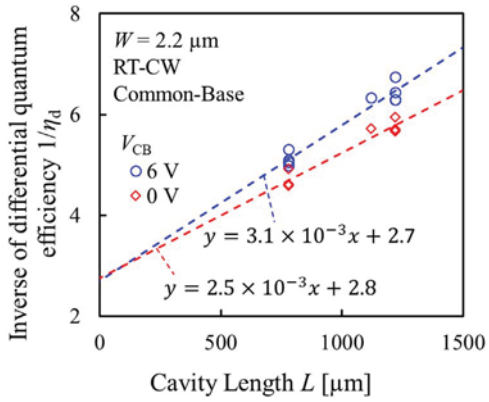

Fig. 6. (Color online) Cavity length dependence of $1/\eta_d$ at different V_{CB} values in the common base configuration.

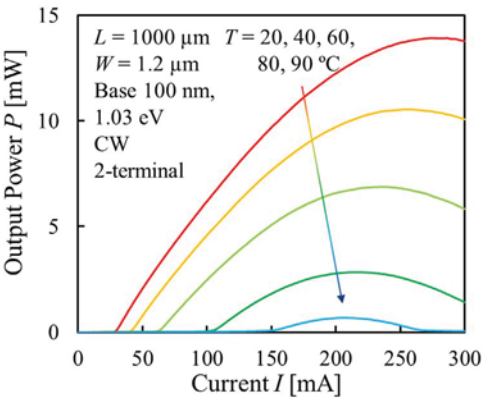

Fig. 8. (Color online) I–P characteristics at various temperatures in a two-terminal configuration.

Acknowledgments

This research was financially supported by the Ministry of Education, Culture, Sports, Science and Technology, (MEXT) KAKENHI Grant Nos.: 17H03247 and 15H05763.

1) T. Ikegami and Y. Suematsu, IEEE J. Quantum Electron. **4**, 148 (1968).
2) R. Nagarajan, T. Fukushima, M. Ishikawa, J. E. Bowers, R. S. Geels, and L. A. Coldren, IEEE Photonics Technol. Lett. **4**, 121 (1992).
3) K. Nakahara, Y. Wakayama, T. Kitatani, T. Taniguchi, T. Fukamachi, Y. Sakuma, and S. Tanaka, IEEE Photonics Technol. Lett. **27**, 534 (2015).
4) J. Shibata, Y. Mori, Y. Sasai, N. Hase, H. Serizawa, and T. Kajiwara, Electron. Lett. **21**, 98 (1985).
5) L. A. Coldren and S. W. Corzine, *Diode Lasers and Photonic Integrated Circuits* (Wiley, New York, 1995).
6) G. Walter, N. Holonyak Jr., M. Feng, and R. Chan, Appl. Phys. Lett. **85**, 4768 (2004).
7) M. Shirao, L. Seung Hun, N. Nishiyama, and S. Arai, IEEE J. Quantum Electron. **47**, 359 (2011).
8) M. J. W. Rodwell, M. Le, and B. Brar, Proc. IEEE **96**, 271 (2008).
9) M. Yukinari, N. Sato, N. Nishiyama, and S. Arai, IEICE Electron. Express **11**, 1 (2014).
10) M. Feng, N. Holonyak, R. Chan, A. James, and G. Walter, Appl. Phys. Lett. **88**, 063509 (2006).
11) M. Shirao, N. Nishiyama, N. Sato, and S. Arai, IEICE Electron. Express **9**, 1792 (2012).
12) C. H. Chang, S. W. Chang, and C. H. Wu, Opt. Express **24**, 25515 (2016).
13) R. Bambery, F. Tan, M. Feng, J. M. Dallesasse, and N. Holonyak Jr, IEEE Photonics Technol. Lett. **25**, 859 (2013).
14) M. Shirao, T. Sato, Y. Takino, N. Sato, N. Nishiyama, and S. Arai, Appl. Phys. Express **4**, 072101 (2011).
15) M. Shirao, T. Sato, N. Sato, N. Nishiyama, and S. Arai, Opt. Express **20**, 3983 (2012).
16) N. Sato, M. Shirao, T. Sato, M. Yukinari, N. Nishiyama, T. Amemiya, and S. Arai, IEEE J. Sel. Top. Quantum Electron. **19**, 6472730 (2013).
17) N. Sato, M. Shirao, T. Sato, M. Yukinari, N. Nishiyama, T. Amemiya, and S. Arai, IEEE Photonics Technol. Lett. **25**, 6471747 (2013).
18) N. Nishiyama, SPIE Photonics Eur. **8**, 10682 (2018).
19) S. Yoshitomi, S. Tadano, K. Yamanaka, N. Nishiyama, and S. Arai, Jpn. J. Appl. Phys. **57**, 012102 (2018).
20) L. J. Qiao, S. Liang, L. S. Han, J. J. Xu, H. L. Zhu, and W. Wang, Opt. Express **23**, 11388 (2015).
21) T. Nakamura, T. Okuda, R. Kobayashi, Y. Muroya, K. Tsuruoka, Y. Ohsawa, T. Tsukuda, and S. Ishikawa, IEEE J. Sel. Top. Quantum Electron. **11**, 141 (2005).
22) S. Yoshitomi, K. Yamanaka, Y. Goto, N. Nishiyama, and S. Arai, 2018 Int. Semiconductor Laser Conf., 2018, p. MC2.
23) C. E. Zah et al., IEEE J. Quantum Electron. **30**, 511 (1994).
24) Y. Yoshida, H. Watanabe, K. Shibata, A. Takemoto, and H. Higuchi, IEEE J. Quantum Electron. **34**, 1257 (1998).
25) R. Gessner, A. Dobbinson, A. Miler, J. Rieger, and E. Veuhoff, J. Cryst. Growth **248**, 426 (2003).
26) Y. Takino, M. Shirao, T. Sato, N. Nishiyama, T. Amemiya, and S. Arai, Jpn. J. Appl. Phys. **50**, 070203 (2011).
27) Y. Takino, M. Shirao, N. Sato, T. Sato, T. Amemiya, N. Nishiyama, and S. Arai, IEEE J. Quantum Electron. **48**, 971 (2012).
28) J. Fu, R. Yang, G. Chen, J. P. Fleurial, and G. J. Snyder, J. Appl. Phys. **104**, 063907 (2008).
29) T. Kaneko, T. Yoshida, S. Tadano, N. Nishiyama, and S. Arai, Jpn. J. Appl. Phys. **55**, 070301 (2016).
30) M. H. MacDougal, J. Geske, C.-K. Lin, A. E. Bond, and P. D. Dapkus, IEEE Photonics Technol. Lett. **10**, 15 (1998).